Linear Waves and Nonlinear Wave Interactions in a Bounded Three-Layer Fluid System

By P. D. Weidman, M. Nitsche, and L. Howard

We investigate possible linear waves and nonlinear wave interactions in a bounded three-layer fluid system using both analysis and numerical simulations. For sharp interfaces, we obtain analytic solutions for the admissible linear mode-one parent/signature waves that exist in the system. For diffuse interfaces, we compute the overtaking interaction of nonlinear mode-two solitary waves. Mathematically, owing to a small loss of energy to dispersive tails during the interaction, the waves are not solitons. However, this energy loss is extremely minute, and because the dispersively coupled waves in the system exhibit the three types of Lax KdV interactions, we conclude that for all intents and purposes the solitary waves exhibit soliton behavior.

1. Introduction

Recently, Nitsche et al. [1] presented a numerical study of mode-two solitary waves traveling on neighboring pycnoclines to determine the range of parameters for which leapfrogging occurs and their ultimate long-time behavior. That work was motivated by the original numerical discovery of leapfrog oscillations by Liu et al. [2] (sometimes denoted LKK in the sequel) for an inviscid fluid and by the laboratory experiments of Weidman and Johnson [3] who observed highly damped leapfrog behavior in a viscous fluid.

Address for correspondence: P. D. Weidman, Department of Mechanical Engineering, University of Colorado, Boulder, CO 80309; e-mail: weidman@colorado.edu.

DOI: 10.1111/j.1467-9590.2011.00540.x

STUDIES IN APPLIED MATHEMATICS 0:1–22

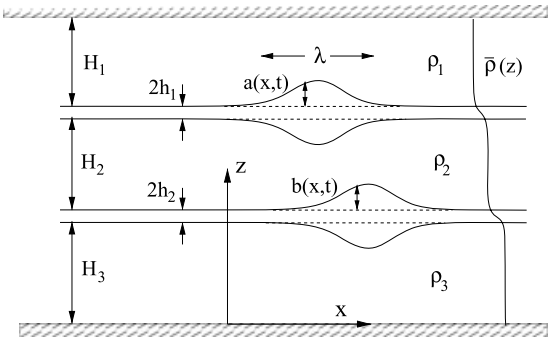

Figure 1. Schematic for nonlinear mode-two wave interactions on neighboring diffuse pycnoclines.

A schematic of the three-layer system studied in [1] is shown in Figure 1 where the origin of the vertical coordinate z lies at the bottom rigid boundary and $z = H_1 + H_2 + H_3 + 2h_1 + 2h_2$ locates the upper rigid boundary. The layers H_1, H_2, and H_3 have constant, stably stratified densities $\rho_1 < \rho_2 < \rho_3$. Transitions between the layers are modeled by hyperbolic tangent profiles of thicknesses $2h_1$ and $2h_2$ as shown in Figure 1. For typical solitary wavelength λ, the LKK equations, valid for $\lambda = O(H_2)$, were solved using an accurate spectral method for the fixed values $H_1 = H_2 = H_3 = 10$ cm, $\rho_1 = 1.02$ g/cm^3, $h_1 = 1.0$ cm and selected values of ρ_2, ρ_3, and h_2. The study shows that leapfrog behavior exists only in a relatively narrow diagonal band of $h_2\Delta\rho_2 - h_1\Delta\rho_1$ space, where $\Delta\rho_1 = \rho_2 - \rho_1$ and $\Delta\rho_2 = \rho_3 - \rho_2$. The initial waveforms were always equal amplitude mode-two Joseph [4] solitary waves. For solutions outside the narrow band, the waves immediately separate and evolve into distinct solitary waves. Solutions within the narrow band oscillate in leapfrog fashion, but during each leap energy is shed into dispersive tails behind the primary waves, thus diminishing their amplitudes continuously over time. The spatial separation between the waves and their oscillation period increase to a point where the waves can no longer communicate, and then they separate into distinct solitary waves.

In this study, we investigate two aspects of this wave system. To orient the reader to the time evolution of travelling waves presented in the coming sections, we show in Figure 2 at dimensionless fixed slow time T, the correspondence between the upper and lower pycnocline deflections Z_U and Z_L and the scaled amplitudes $A(\xi, T)$ and $B(\xi, T)$ in a frame of reference $\xi = x - c_0 t$ moving with the average linear wave speed. Figure 2 shows a case when the leapfrog motion has ceased and the waves are separating in time due to their different celerities. These are steady solitary waves: they propagate without change of form and at constant speed. In Figure 2(a), the pycncoline deflections Z_U and Z_L are plotted without magnification and in Figure 2(b) they are

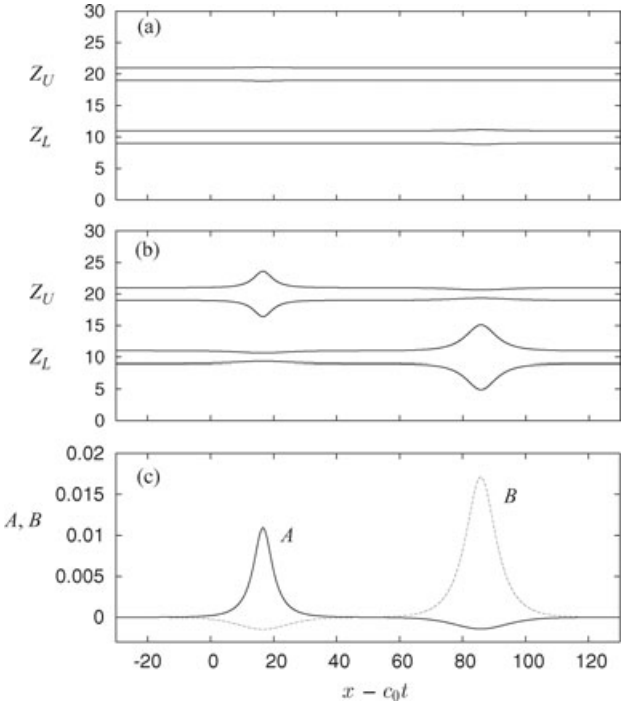

Figure 2. Upper Z_U and lower Z_L pycnocline deflections shown (a) without magnification and (b) with 25-X magnification for separated solitary waves. The normalized wave amplitudes $A(\xi, T)$ on the upper pycnocline and $B(\xi, T)$ on the lower pycnocline with $\xi = x - c_0 t$ are shown in (c) by the solid and dashed lines, respectively.

seen with 25-fold magnification. In Figure 2(c), the pycnocline disturbances characterized by $A(\xi, T)$ (solid line) on the upper pycnocline and $B(\xi, T)$ (dashed line) on the lower pycnocline are displayed. It is clear that each parent mode-two solitary wave of elevation on one pycnocline is always accompanied by a phase-locked mode-two signature wave of depression on its neighboring pycnocline. The first aspect of this study is to determine the possible linear parent and signature waves that co-exist in a three-layer system with sharp density interfaces. For density jumps $\Delta\rho_1$ and $\Delta\rho_2$ typical of laboratory conditions, will the signature wave always have a deflection opposite that of the parent wave in the linear sharp-interface system?

The second part of this study is to determine whether the separated solitary waves found in [1] are indeed solitons. That is, do overtaking waves along a single pycnocline in the two pycnocline system emerge from an interaction without change of speed or form, but with only a spatial phase shift? And how do the interactions compare to classical KdV interactions?

The presentation is as follows. The study of linear waves in a three-layer system with sharp density interfaces is presented in Section 2. The numerical

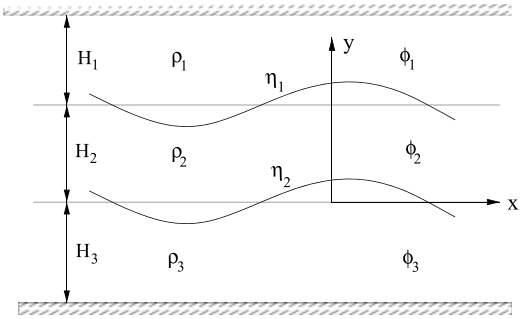

Figure 3. Schematic for linear waves in a sharp two-pycnocline system.

study of overtaking solitary waves in a three-layer system with diffuse density interfaces is presented in Section 3. A summary and concluding remarks are given in Section 4.

2. Linear waves on sharp density interfaces

Lamb [5] has given the waveforms and frequencies for linear standing waves in the following situations: (1) waves on the free surface of fluid of depth H_1; (2) waves on the liquid–liquid interface of a two-layer system of depths H_1 and H_2 bounded by rigid walls top and bottom; and (3) waves on the free and liquid–liquid interfaces of a two-layer system of depths H_1 and H_2 bounded by a lower rigid wall. Clearly, for such sharp interfaces, only mode-one waves are possible. We now extend Lamb's results to the case (4) of interface motions in a three-layer system bounded above and below by rigid walls. The schematic of the system is given in Figure 3. We take three layers which, top to bottom, have thicknesses H_1, H_2, H_3 with associated statically stable densities $\rho_1 < \rho_2 < \rho_3$. Following Lamb [5], it is convenient to place the origin of the vertical y-coordinate at the undisturbed lower interface, so $y = -H_3$ is the bottom wall, $y = \eta_2$ is the lower interface, $y = H_2 + \eta_1$ is the upper interface and $y = H_2 + H_1$ is the upper wall. For potential function ϕ defined by $\mathbf{u} = \nabla\phi$, we must satisfy Laplace's equation

$$\nabla^2\phi = 0 \qquad \text{in} \qquad \mathcal{D}, \tag{1}$$

where $\mathcal{D}$ is the quiescent fluid domain.

Assumed forms of the potential functions in the three layers that satisfy impermeability at the upper and lower boundaries are taken as

$$\phi_1 = D\cosh k\,(y - H_1 - H_2)\cos kx\,\mathrm{e}^{\mathrm{i}\sigma t} \tag{2a}$$

$$\phi_2 = (A\cosh ky + B\sinh ky)\cos kx\,\mathrm{e}^{\mathrm{i}\sigma t} \tag{2b}$$

$$\phi_3 = C \cosh k\,(y + H_3) \cos kx\, \mathrm{e}^{\mathrm{i}\sigma t}. \tag{2c}$$

The deflections for standing waves on the lower and upper interfaces are, respectively,

$$\eta_2 = a \cos kx\, \mathrm{e}^{\mathrm{i}\sigma t}, \qquad \eta_1 = b \cos kx\, \mathrm{e}^{\mathrm{i}\sigma t}, \tag{3a,b}$$

where k is the wavenumber and σ is the frequency of the waves. In what follows we will consider $\eta_2(x, t)$ the parent wave and $\eta_1(x, t)$ its signature wave; thus in (3a,b) the amplitude a is given and the amplitude b is to be determined.

At the linearized position of each interface, we have the kinematic (continuity of velocity) and dynamic (continuity of pressure) conditions across the interface. Consequently, at the lower interface one must satisfy

$$\left.\begin{aligned} \frac{\partial \eta_2}{\partial t} &= \frac{\partial \phi_3}{\partial y}, \qquad & \frac{\partial \eta_2}{\partial t} &= \frac{\partial \phi_2}{\partial y} \\ \rho_2 \left(\frac{\partial \phi_2}{\partial t} + g\,\eta_2 \right) &= \rho_3 \left(\frac{\partial \phi_3}{\partial t} + g\,\eta_2 \right) \end{aligned}\right\} \qquad (y = 0) \tag{4a,b,c}$$

and at the upper interface

$$\left.\begin{aligned} \frac{\partial \eta_1}{\partial t} &= \frac{\partial \phi_2}{\partial y}, \qquad & \frac{\partial \eta_1}{\partial t} &= \frac{\partial \phi_1}{\partial y} \\ \rho_2 \left(\frac{\partial \phi_2}{\partial t} + g\,\eta_1 \right) &= \rho_1 \left(\frac{\partial \phi_1}{\partial t} + g\,\eta_1 \right) \end{aligned}\right\} \qquad (y = H_2). \tag{5a,b,c}$$

We now proceed to determine the unknown constants. Applying kinematic conditions (4a,b) at the lower interface gives

$$B = \frac{\mathrm{i}\sigma a}{k}, \qquad C = \frac{\mathrm{i}\sigma a}{k \sinh k H_3} \tag{6a,b}$$

and continuity of pressure (4c) across that interface furnishes the relation

$$\rho_2(\mathrm{i}\sigma A + ga) = \rho_3(\mathrm{i}\sigma C \cosh k H_3 + ga). \tag{7}$$

Applying kinematic conditions (5a,b) at the upper interface gives

$$D = -\frac{\mathrm{i}\sigma b}{k \sinh k H_1}, \qquad A \sinh k H_2 + B \cosh k H_2 = \frac{\mathrm{i}\sigma b}{k} \tag{8a,b}$$

and continuity of pressure (5c) across that interface yields

$$\rho_2[\mathrm{i}\sigma(A \cosh k H_2 + B \sinh k H_2) + gb] = \rho_1[\mathrm{i}\sigma D \cosh k H_1 + gb]. \tag{9}$$

For fixed lower interface amplitude a we have A, B, C, D, σ, and b as unknowns. Inserting (6b) into (7) gives

$$A = \frac{a}{i\sigma} \left[-\chi \frac{\sigma^2}{k} \coth_3 + (\chi - 1) g \right] \tag{10}$$

in which we have adopted the shorthand notation

$$\chi = \frac{\rho_3}{\rho_2}, \qquad \coth_n = \coth kH_n. \tag{11}$$

Now inserting (6a), (8a), and (10) into Equation (9) yields

$$\left[-\chi\frac{\sigma^2}{k}\coth_3 + (\chi - 1)g\right]\cosh kH_2 - \frac{\sigma^2}{k}\sinh kH_2 + g\alpha$$
$$= \gamma\left[\frac{\sigma^2}{k}\coth_1 + g\right]\alpha, \tag{12}$$

where the additional shorthand notations

$$\alpha = \frac{b}{a}, \qquad \gamma = \frac{\rho_1}{\rho_2} \tag{13}$$

are adopted. To obtain another equation relating α and σ^2, the expressions for A in (10) and B in (6a) are inserted into Equation (8b) to find

$$[-\chi\beta\coth_3 + (\chi - 1)]\sinh kH_2 - \beta\cosh kH_2 = -\alpha\beta, \tag{14}$$

where now

$$\beta = \frac{\sigma^2}{gk}. \tag{15}$$

Dividing (12) by g and introducing the dimensionless frequency β yields

$$[-\chi\beta\coth_3 + (\chi - 1)]\cosh kH_2 - \beta\sinh kH_2 = \alpha[(\gamma - 1) + \gamma\beta\coth_1]. \tag{16}$$

The solution of (14) and (16)

$$\alpha = \frac{[\chi\beta\coth_3 - (\chi - 1)]\sinh kH_2 + \beta\cosh kH_2}{\beta}$$
$$= \frac{[-\chi\beta\coth_3 + (\chi - 1)]\cosh kH_2 - \beta\sinh kH_2}{[(\gamma - 1) + \gamma\beta\coth_1]} \tag{17}$$

furnishes two separate equations for the amplitude ratio. Now divide both sides of this expression by $\sinh kH_2$ to obtain a quadratic equation for β, *viz.*

$$[\gamma\chi\coth_1\coth_3 + \gamma\coth_1\coth_2 + \chi\coth_2\coth_3 + 1]\beta^2$$
$$- [(\chi - \gamma)\coth_2 + \chi(1 - \gamma)\coth_3 + \gamma(\chi - 1)\coth_1]\beta$$
$$+ [(\chi - 1)(1 - \gamma)] = 0. \tag{18}$$

The statically stable density ratios satisfy $\chi > 1$ and $0 < \gamma < 1$. Each of the terms inside the square brackets are positive because each $\coth_n$ function is positive. One can readily show that (18) reduces, in the limit $\gamma \to 0$, to Lamb's eigenvalue problem for two fluid layers with an upper free surface.

2.1. Amplitude ratio

We seek the simplest expression for the amplitude ratio as in Lamb [5]. To do this, we first solve for χ in (18) to obtain

$$\chi = -\frac{\gamma(\beta\coth_2+1)(\beta\coth_1+1)+(\beta^2-1)}{(\beta\coth_3-1)[\gamma(\beta\coth_1+1)+(\beta\coth_2-1)]}. \tag{19}$$

Inserting this into the first expression for α in (17) and simplifying gives

$$\alpha = \frac{\beta}{\sinh kH_2\,[\gamma(\beta\coth_1+1)+(\beta\coth_2-1)]}. \tag{20}$$

Lamb's result for the two-layer system with a free surface is obtained by setting $\gamma = 0$, but for the three-layer system with rigid upper and lower surfaces the additional term $\gamma(\beta\coth_1+1)$ appears in the bracket in the denominator. Evidently, one cannot eliminate both density ratios χ and γ in favor of β for this three-layer system.

Two example solutions will now be presented, one for equal density jumps across the pycnoclines and the other for disparate density jumps. In each case, we provide results for fluid depths $H_1 = H_2 = H_3 = 15$ cm and choose the wavelength $\lambda = 45$ cm.

Equal density jumps

Using the layer densities

$$\rho_1 = 1.02, \quad \rho_2 = 1.05, \quad \rho_3 = 1.08 \text{ (g/mL)},$$

one finds the amplitude ratios and dimensionless frequencies

$$\begin{aligned} \alpha_1 &= 1.124668, & \beta_1 &= 0.015787 \\ \alpha_2 &= -0.889152, & \beta_2 &= 0.012350. \end{aligned}$$

Thus, for α_1, the signature wave deflects in the same direction as the parent wave whereas for α_2, they deflect oppositely. This is seen in Figure 4 where the parent wave η_2 on the lower pycnocline is shown with its in-phase signature wave η_1^+ and its out-of-phase signature wave η_1^-.

Unequal density jumps

We now present a calculation for different density jumps using the densities

$$\rho_1 = 1.02, \quad \rho_2 = 1.11, \quad \rho_3 = 1.167 \text{ (g/mL)}.$$

For this disparate density jump configuration, we find the amplitude ratios and dimensionless frequencies

$$\begin{aligned} \alpha_1 &= 3.620907, & \beta_1 &= 0.042474 \\ \alpha_2 &= -0.174910, & \beta_2 &= 0.023793. \end{aligned}$$

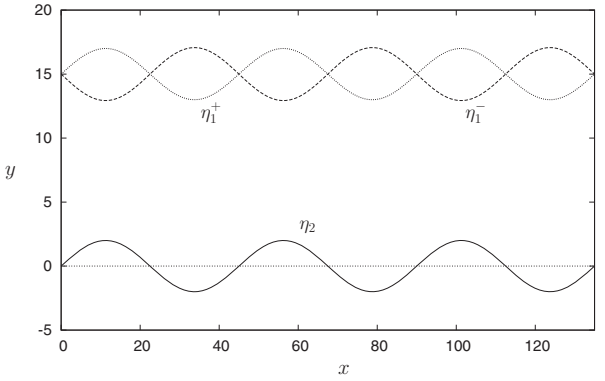

Figure 4. Parent wave η_2 shown with accompanying in-phase signature wave η_1^+ and out-of-phase signature wave η_1^- for the equal density jump example.

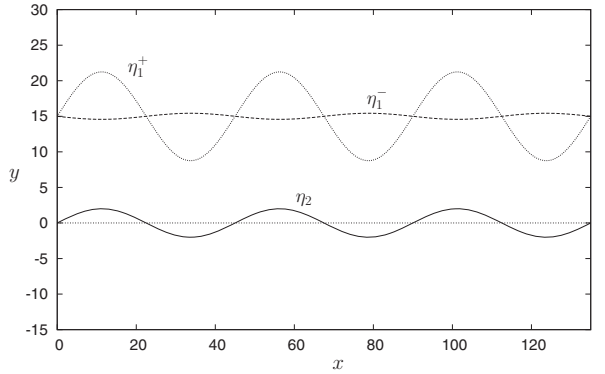

Figure 5. Parent wave η_2 shown with accompanying in-phase signature wave η_1^+ and out-of-phase signature wave η_1^- for the unequal density jump example.

In this example the plot over the full height of the tank, with upper wall at $y = 30$ cm and lower wall at $y = -15$ cm, is shown in Figure 5.

2.2 Equal amplitude parent and signature waves

Another query concerns whether equal amplitude parent and signature waves can co-exist. A necessary condition for the existence of such parent/signature waves may be obtained by setting $\alpha = \pm 1$ in (2.20) and solving for β. The result is

$$\beta = \frac{\pm(1-\gamma)\sinh kH_2}{\pm(\gamma\coth_1 + \coth_2)\sinh kH_2 - 1}, \tag{21}$$

where the plus (minus) sign corresponds to in-phase (out-of-phase) signature wave. This result must be compatible with one of the two solutions of

Equation (18), so we insert (21) into (18) to obtain the criterion for equal amplitude parent/signature waves, *viz.*

$$(1-\gamma)(1-\coth_2^2)\sinh^2 kH_2 \quad + [(2-\gamma-\chi)\coth_2 + \chi(1-\gamma)\coth_3 - (\chi-1)\gamma\coth_1](\pm\sinh kH_2) + (\chi-1) = 0. \tag{22}$$

This is a relation, for fixed wavenumber k, between the fluid thicknesses and their densities. As an example application, consider the following laboratory experiment. A long rectangular tank is available with a total 40 cm depth between the bounding horizontal walls. An experimentalist lays in the bottom two layers H_2 and H_3 with respective densities ρ_2 and ρ_3. He/she is then left with deciding what density for the remaining layer of thickness H_1 is required to see a signature wave on the upper interface with the same amplitude as the parent wave on the lower interface. Solving Equation (22) for the density ratio γ furnishes the desired result

$$\gamma = \frac{(\coth_2^2 - 1)\sinh^2 kH_2 - [2\coth_2 + \chi(\coth_3 - \coth_2)](\pm\sinh kH_2) - (\chi-1)}{(\coth_2^2 - 1)\sinh^2 kH_2 - [\coth_2 - \coth_1 + \chi(\coth_3 + \coth_1)](\pm\sinh kH_2)}. \tag{23}$$

We now provide two examples where parent and signature waves have equal amplitudes. In the first example, the equal amplitude signature wave is in-phase with the parent wave and, therefore, the parent and signature waves are identical. In the second example, the equal amplitude signature wave is out-of-phase with the parent wave.

Identical parent and signature waves

For the laboratory experiment, two bottom layers in a 40-cm-deep channel are laid in as follows

$$\rho_2 = 1.05, \qquad \rho_3 = 1.10 \text{ (g/mL)}$$
$$H_2 = 20.0, \qquad H_3 = 10.0 \text{ (cm)}.$$

To observe an identical in-phase signature wave on the upper interface, the only remaining unknown is the density ρ_1 of the uppermost 10-cm layer. This is obtained by solving for γ using the positive sign in Equation (23). One thereby finds $\gamma = 0.954796$ which gives $\rho_1 = 1.002536$ g/mL. The amplitude ratios and dimensionless frequencies for this example are

$$\alpha_1 = 1.000000, \qquad \beta_1 = 0.023017,$$
$$\alpha_2 = -1.053455, \qquad \beta_2 = 0.020513,$$

with waveforms shown in Figure 6.

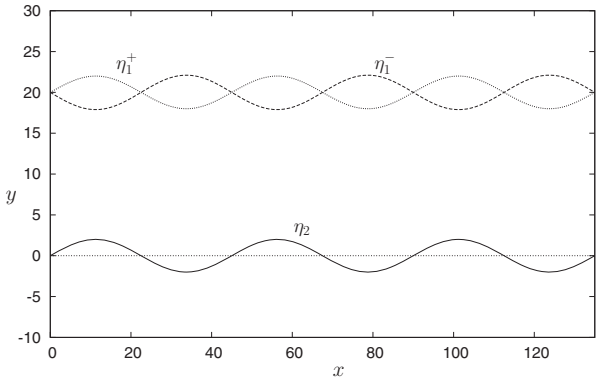

Figure 6. Parent wave η_2 shown with its identical signature wave η_1^+ and the out-of-phase signature wave η_1^- of unequal amplitude.

Equal amplitude out-of-phase parent and signature waves

For the same parameters as in the previous section, we now choose the minus sign in Equation (23) to find $\gamma = 0.954545$ which gives $\rho_1 = 1.002273$ g/mL. The amplitude ratios and dimensionless frequencies for this case are

$$\begin{aligned} \alpha_1 &= 1.047627, & \beta_1 &= 0.023082, \\ \alpha_2 &= -1.000000, & \beta_2 &= 0.0205271. \end{aligned}$$

2.3 Equal amplitude signature waves

Finally, one can ask whether, for a particular parent wave, equal amplitude signature waves can exist, either in-phase or out-of-phase with the parent wave. The criterion for this possibility is obtained by setting Equation (20) equal to the negative of itself. This gives the requirement

$$\beta = \frac{1-\gamma}{(\gamma \coth_1 + \coth_2)}. \tag{24}$$

Inserting this into the frequency Equation (18) furnishes the simple criterion

$$\coth_2 \equiv \coth kH_2 = 1. \tag{25}$$

Thus equal amplitude signature waves are obtained, for any wavenumber k, only in the limit where the middle layer is infinitely deep.

3. Overtaking solitary waves on diffuse interfaces

In the second part of our study, we consider the overtaking interaction of mode-two solitary waves on the upper pycnocline in a three-layer system with diffuse interfaces. The liquid depths H_i, densities ρ_i and pycnocline thicknesses h_j are defined in Figure 1. The diffusively coupled KdV equations for scaled amplitudes $A(\xi, T)$ and $B(\xi, T)$ originally formulated in [2], and carefully rederived in [1], are

$$A_T - \Delta A_\xi + \alpha_1 A A_\xi + \beta_1 \frac{\partial^2}{\partial \xi^2} [\mathcal{H}_1(A) + \mathcal{H}_2(A) + \mathcal{H}(B)] = 0 \quad (26a)$$

$$B_T + \Delta B_\xi + \alpha_2 B B_\xi + \beta_2 \frac{\partial^2}{\partial \xi^2} [\mathcal{H}_3(B) + \mathcal{H}_2(B) + \mathcal{H}(A)] = 0, \quad (26b)$$

where $\mathcal{H}$ and $\mathcal{H}_j$ are Hilbert operators. The coefficients of nonlinearity $\alpha_{1,2}$ and of dispersion $\beta_{1,2}$ are given by

$$\alpha_{1,2} = \frac{3}{2} \frac{\int_{U,L} \overline{\rho}(\phi'_{1,2})^3 \, dz}{\int_{U,L} \overline{\rho}(\phi'_{1,2})^2 \, dz}, \qquad \beta_{1,2} = \frac{1}{2} \frac{c_{1,2}\rho_2}{\int_{U,L} \overline{\rho}(\phi'_{1,2})^2 \, dz}, \quad (27)$$

in which $\phi_{1,2}$ are the linear mode-two eigenfunctions associated with the upper (U) and lower (L) pycnoclines, respectively. The associated linear long-wave speeds are $c_{1,2} = c_0 \pm \Delta$, which serves to define both c_0 and Δ. The spatial variable is $\xi = x - c_0 t$ and $T = \epsilon t$ is a slow time. All variables are nondimensionalized using h_1 and $(h_1/g)^{1/2}$ as length and time scales, where g is gravity.

The lowest nontrivial $\phi_{1,2}(z)$ modes are called *mode-two* waves, since on each pycnocline, the stream function amplitudes at the top and bottom boundaries are $\pm A$ and $\pm B$, respectively. It is pertinent to note that a *mode-one* solution of the eigenvalue equation is technically allowed, namely $\phi_{1,2}(z)$, but the speed is infinite since the corresponding eigenvalue is $1/c_{1,2}^2 = 0$, and so such modes are excluded.

The system (26) conserves the total energy

$$\mathcal{E}(T) = \frac{1}{2} \int_{-\infty}^{\infty} \left(\frac{A^2(\xi, T)}{\beta_1} + \frac{B^2(\xi, T)}{\beta_2} \right) d\xi. \quad (28)$$

It was shown in Nitsche et al. [1] that the numerical method used to solve this system conserves energy to within a small fraction of the filtered energy.

It was not shown in Nitsche et al. [1] whether the separated solitary waves were solitons. The goal here is to perform numerical experiments for overtaking solitary waves to determine to what extent the postinteraction waves replicate the preinteraction waves in form and speed, and to see whether the

only remnant of the interaction is a spatial phase shift in wave trajectories, this being the definition of a soliton. We also want to determine whether the overtaking interaction is similar to the classic KdV interaction.

The exact solution of the KdV equation for multiple soliton collisions was first given by Hirota [6] and is discussed in detail by Whitham [7] for the case of an interaction between two solitary waves. We recall the three types of overtaking KdV interactions found by Lax [8] who defined the amplitude ratio $\sigma = a_1/a_2 > 1$, where a_1 is the peak amplitude of the larger trailing wave and a_2 is the peak amplitude of the smaller lead wave. For the Type I interaction in the range $1 < \sigma < (3 + \sqrt{5})/2$, the wave peaks remain distinct with a continuous decrease (increase) in the amplitude of the trailing (leading) wave; the mid-interaction waveform is symmetric with two maxima. For the Type III interactions in the range $\sigma > 3$, the trailing wave simply rides over the lead wave so the mid-interaction waveform is characterized by a single maximum. The small range $(3 + \sqrt{5})/2 < \sigma < 3$ corresponds to the Type II interaction. Here, the faster wave tries to engulf the slower one, and in fact the smaller amplitude lead wave loses its crest only to regain it before the middle of the interaction; as for the Type I interaction, the mid-interaction waveform is symmetric with two maxima. The theory [6] shows that in every case, the larger wave experiences a forward spatial shift whereas the smaller wave undergoes a backward spatial shift as a result of the interaction. These KdV interactions have been verified for water waves propagating on a layer of uniform depth in a long channel by Weidman and Maxworthy [9] where special corrections had to be made to remove the effect of viscous wave attenuation.

For this study, we take equal depths $H_1 = H_2 = H_3 = 15$ cm, densities $\rho_1 = 1.02$, $\rho_2 = 1.11$, $\rho_3 = 1.167$ g/mL, and pycnocline half-thicknesses $h_1 = 1.0$ cm and $h_2 = 1.8$ cm. For these parameters, integration of the linear eigenvalue equations yields the eigenfunctions $\phi_{1,2}(z)$ with dimensionless linear wave speeds $c_1 = 3.219$ and $c_2 = 3.323$ from which the coefficients $\alpha_1 = 2.35$, $\alpha_2 = 1.35$, $\beta_1 = 0.657$, and $\beta_2 = 1.067$ are calculated. We first compute solitary wave solutions to (26) for a range of peak amplitudes. Each of these consists of an elevation wave $A(\xi, t)$ on the upper pycnocline with a phase-locked depression wave $B(\xi, T)$ on the lower pycnocline which translate together with constant speed, without change of shape or energy. These steady states are computed by evolving an approximately steady initial condition obtained from rescaled results in [1]. The initial wave sheds a tail of dispersive waves which is removed by a numerical filter from the periodic domain until the shape and speed become constant. As explained in [1], the filter removes energy from the computational domain; however, the sum of the filtered energy and the remaining energy in the domain remains unchanged to within 0.01%. The results are steady in a moving reference frame except for background noise of relative magnitude $\leq 10^{-8}$.

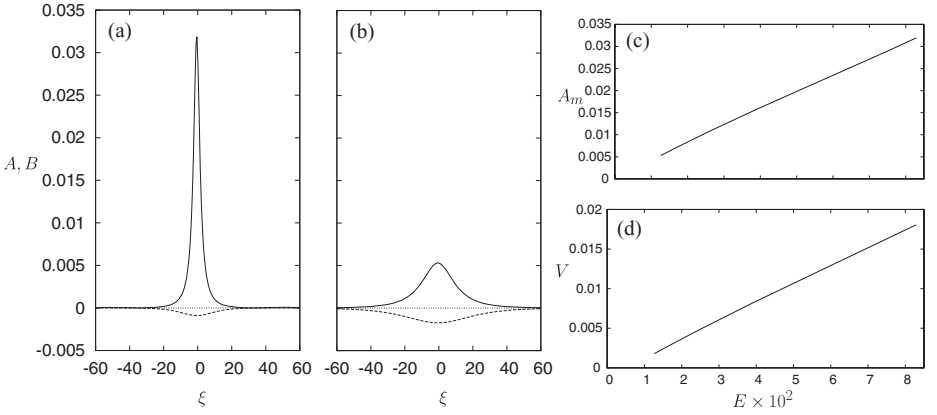

Figure 7. Steady solitary wave solutions with (a) amplitude $A1_0 = 1$, (b) amplitude $A1_0 = 0.12$. Relation between (c) amplitude and energy, and (d) speed and energy of the steady solitary wave solutions.

Figures 7(a) and (b) show two computed steady solitary waves, one with peak amplitude $A_0 = 1$, the other with $A_0 = 0.12$. For smaller amplitude A-waves, the depression B-wave is larger relative to the A-wave, and the shape is broader. The steady state energies are a continuous function of their peak amplitude A_m and of their speed V as shown in Figures 7(c) and (d). The energy tends to zero as the amplitude tends to zero; however, because $V = d\xi/dT$ is the speed in the moving reference frame, the energy goes to zero at $V = -\epsilon c_0$, where $T = \epsilon t$ is the slow time variable. This data will be used in the sequel to determine wave energies from their speed and amplitude, in cases when the energy is difficult to compute directly. For the overtaking wave interaction, the initial condition consists of a superposition of mode-two solitary waves, a larger wave of peak amplitude $A1_0 = 1$ propagating towards a slower wave of amplitude $A2_0 < A1_0$ and we define the amplitude ratio $\sigma = A1_0/A2_0$. The waves are sufficiently separated so that there is no initial interaction between them. The subsequent time evolution is computed using the pseudo-spectral method described in [1], with L=1000, N=4096, $\Delta t = 0.005$. Figure 8 shows the waveform evolution for three different amplitude ratios $\sigma = 2.33$, 3.92, and 5.07. These values of σ exhibit interaction waveforms typical of the KdV Type I, II, and III interactions.

The three interactions can be easily distinguished by plotting the time evolution of the peak amplitudes $A1_m$, $A2_m$ and their corresponding trajectories $X_{A1}(T)$, $X_{A2}(T)$. Figure 9 shows the results for the same values of σ used in Figure 8. In the left column, the evolution of $A1_m$ is shown by the solid line and the evolution of $A2_m$ is shown by the dotted line. Similarly, in the right column, the trajectory of $A1_m$ is shown by the solid line and that of $A2_m$ is shown by the dotted line.

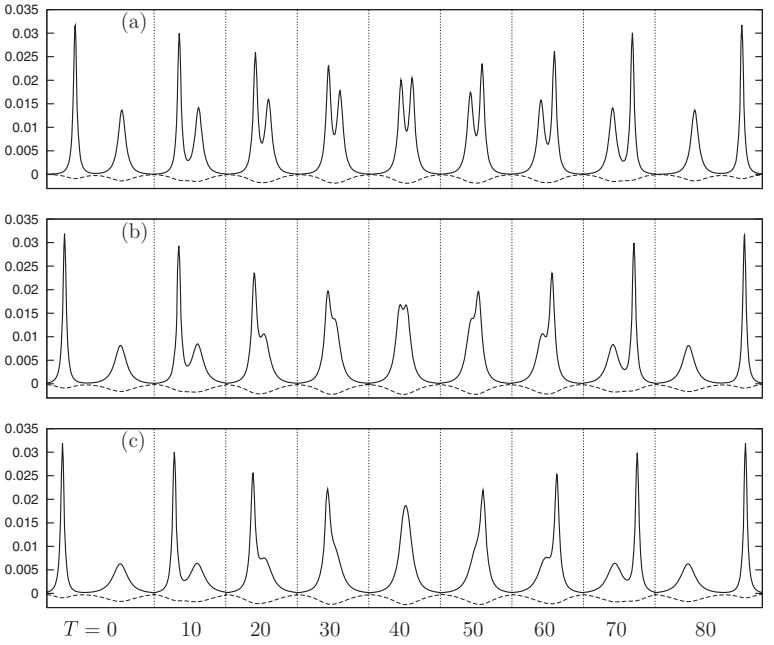

Figure 8. Waveform evolutions for three different amplitude ratios. Panel (a) for $\sigma = 2.33$ is typical of a Type I KdV interaction; panel (b) for $\sigma = 3.92$ is typical of a Type II KdV interaction; and panel (c) for $\sigma = 5.07$ is typical of a Type III KdV interaction.

The top row in Figure 9 is typical of the Type I interaction where the peak amplitudes continuously rise and fall whereas their trajectories remain distinct, and the mid-interaction profile is symmetric with two maxima as in Figure 8(a). The middle row corresponds to the intricate Type II interaction where during a brief period, before and after the middle of the interaction, a wave loses its peak, yet the mid-interaction profile is symmetric with two maxima as in Figure 8(b). The bottom row corresponds to the Type III interaction where the trailing wave simply overrides the lead wave in which case the symmetric mid-interaction profile consists of a single maximum as in Figure 8(c).

After each interaction, the waves approach constant translation speed, evidenced by the linear trajectories in the right column of Figure 9. These figures also show dashed lines which are continuations of the linear preinteraction trajectories. These lines appear to be parallel to the postinteraction trajectories, indicating that wave celerity remains unchanged by the interaction.

If the final speeds and amplitudes were equal to the initial ones, as is the case for true solitons, then the phase shifts would be time-independent. In that case, the forward spatial phase shifts of the $A1$-waves would be ΔX_1 and the backward spatial phase shifts of the $A2$-waves would be ΔX_2 as indicated in Figure 9. However, we detect very small energy losses as a result of

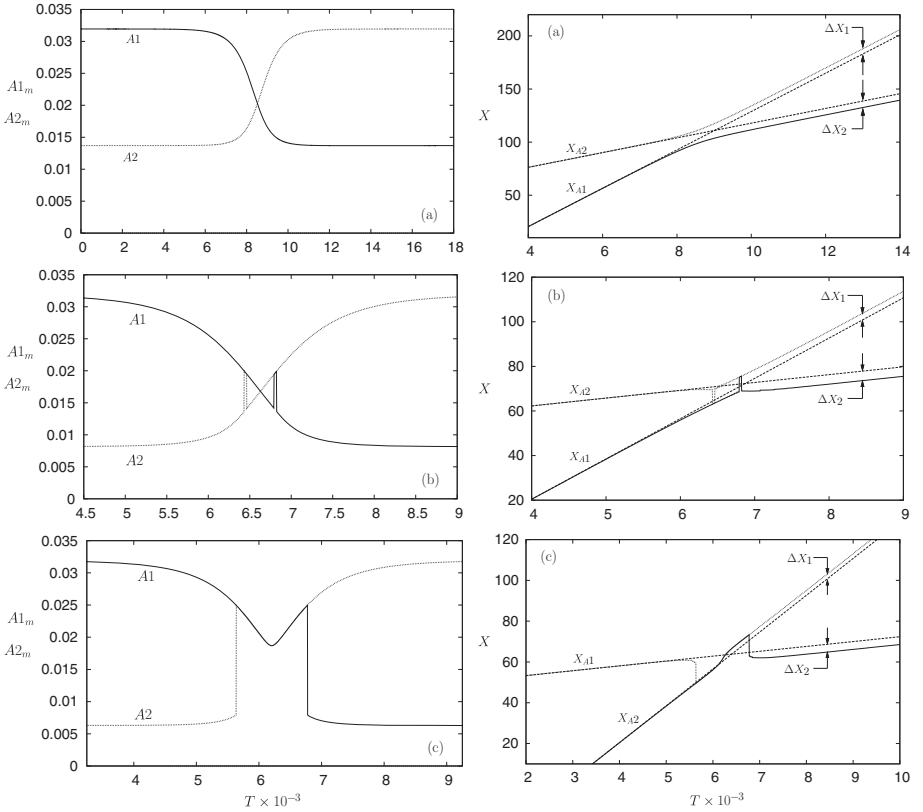

Figure 9. Time evolution of peak wave amplitudes $A1_m$ and $A2_m$ and space–time trajectories of those peak amplitudes for (a) Type I interaction at $\sigma = 2.33$, (b) Type II interaction at $\sigma = 3.92$, and (c) Type III interaction at $\sigma = 5.07$.

these interactions. Figure 10 shows the waveforms before and after a Type I interaction at $\sigma = 2.50$, on three different scales. The top row shows the pre- and postinteraction waveforms without magnification. The middle row shows the same results with $\times 100$ magnification; here one first discerns energy being released from the A-wave of elevation and the B-wave of depression into dispersive tails on the separated pycnoclines. Note that the amplitude of the dispersive tails is much smaller than even the small phase-locked B depression wave. In the bottom row shown at $\times 1000$ magnification, full details of the dispersive tails are exhibited.

We find that the two emerging solitary waves travel with slightly changed energy, speed and amplitude. To illustrate the actual amount of energy lost, Figure 11(a) shows the change $\Delta E_{1,2}$ in the $A1$- and $A2$-waves, relative to their initial energies $E_{1,2}$. The change in the total solitary wave energies $E = E_1 + E_2$ can be measured directly only when the evolution

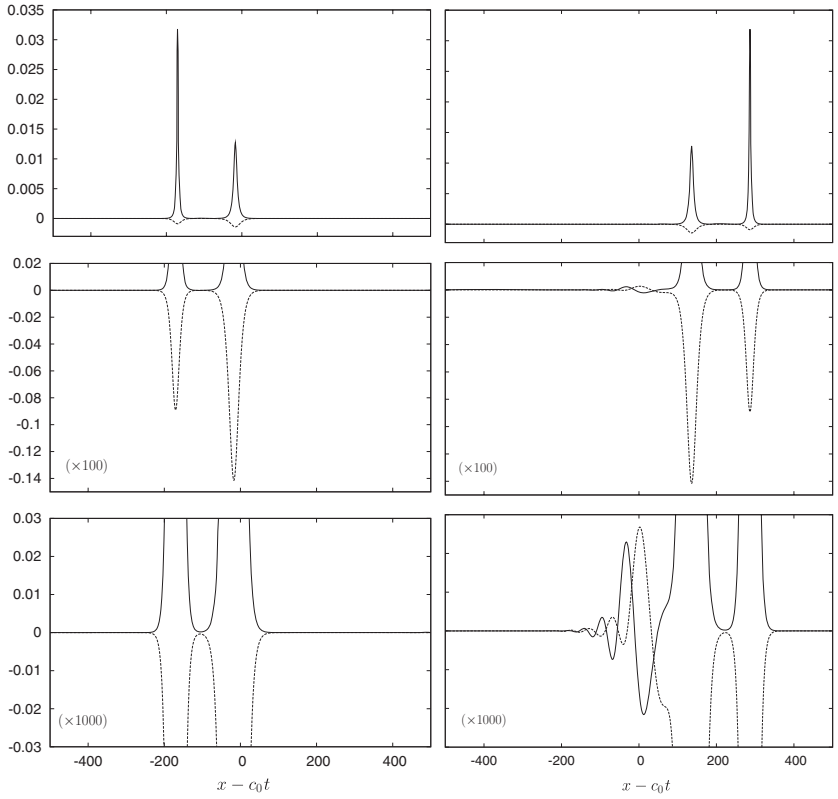

Figure 10. Waveforms before (left column) and after (right column) a Type I interaction at $\sigma = 2.50$ showing details of the dispersive waves generated at three different magnifications.

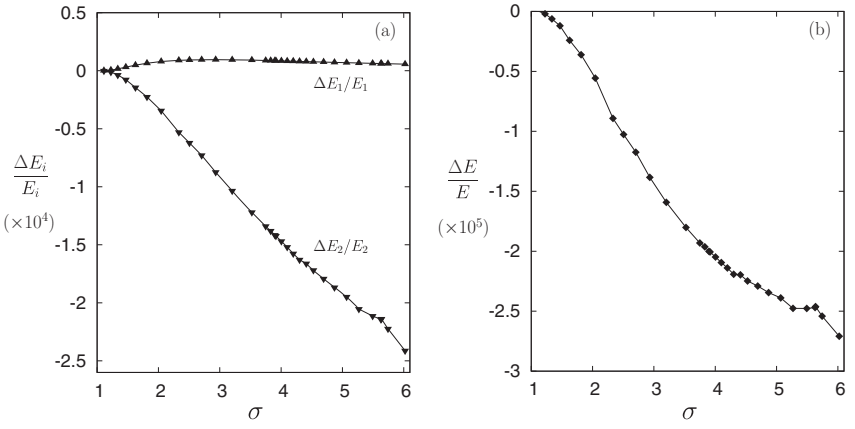

Figure 11. Pre- and postinteraction energy changes as a function of σ; (a) $\Delta E_1/E_1$ and $\Delta E_2/E_2$ and (b) $\Delta E/(E)$, where $E_{1,2}$ are the energies in the $A1$- and $A2$-waves, respectively.

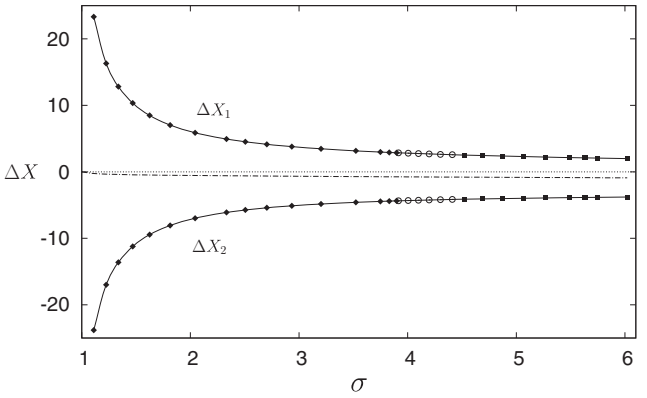

Figure 12. Forward phase shifts ΔX_1 of the $A1$-waves and rearward shifts ΔX_2 of the $A2$-waves as a function of σ. Solid diamonds denote Type I interactions, open circles denote Type II interactions, and solid squares denote Type III interactions. The dash-dot-dash curve is the average of the forward and rearward phase shifts.

can be computed for sufficiently long time that all dispersive tails leave the computational domain through the filter. Because of the finite size of the domain and the increasing distance between the two solitary waves, this was only possible for small values of σ. At larger values of σ, we obtained the changes $\Delta E_{1,2}$ by measuring the asymptotic speed and amplitude of each wave and using the relations in Figures 7(c) and (d) to deduce the corresponding wave energy. The results were consistent with each other and with direct computation of the total energy change, when available.

However, there was some uncertainty for large ratios σ, because in these cases the slow waves approached their steady states very slowly. The oscillations in Figures 11(a) and (b) near $\sigma = 5.5$ are attributed to such estimation errors.

Figure 11(a) shows that the initially large amplitude $A1$-wave actually gains up to 0.001% energy during the interaction, whereas the initially small amplitude $A2$-wave loses up to 0.025% of its energy for the values of σ considered. Figure 11(b) shows the resulting loss in the sum of the energies of the solitary wave system, $\Delta E/E$. At high σ as much as 0.003% energy is lost from the solitary waves to their dispersive tails.

These values capture the magnitude of the differences between pre- and postinteraction wave speeds and show that the postinteraction trajectories on the right column in Figure 9 are not identically parallel to the preinteraction trajectories. As a result the phase shifts $\Delta X_{1,2}$ shown in Figure 9 are not constant but depend ever so slightly on time. We define the phase shifts to be the values of $\Delta X_{1,2}$ at $T = T_{\text{mid}}$, where T_{mid} denotes the middle of the interaction. These phase shifts are displayed in Figure 12. As illustrated by the three different symbols, we find that Type I interactions occur in the range

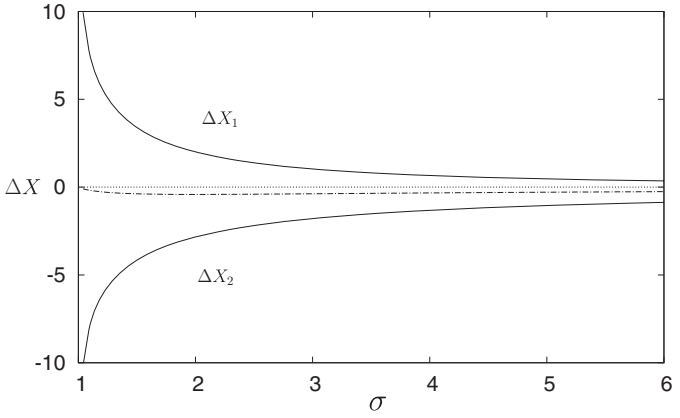

Figure 13. Forward phase shifts ΔX_1 and rearward phase shifts ΔX_2 for a KdV interaction of free surface waves as a function of σ. The dash-dot-dash curve is the average of the forward and rearward phase shifts.

$0 < \sigma < 3.9$, Type II interations appear in the range $3.9 < \sigma < 4.45$, and Type III interactions are found for $\sigma > 4.45$. The dash–dot–dash line near $\Delta X = 0$ in Figure 12 is the average of the two curves. The average tends to zero as $\sigma \to 0$ and decreases linearly at high σ in the range of sigma displayed.

For comparison, we compare our spatial phase shifts with those for a KdV interaction of solitary water waves propagating over a liquid layer of uniform depth h_0 given by

$$\Delta X_i = \frac{\Delta X_i^*}{h_0} = \pm \frac{2}{(3\alpha_i)^{1/2}} \ln\left(\frac{\sigma^{1/2}+1}{\sigma^{1/2}-1}\right), \tag{29}$$

in which $\alpha_i = a_i/h_0$ are the dimensionless peak amplitudes and ΔX_i^* are the dimensional spatial phase shifts. For the results presented in Figure 13, we choose $\alpha_2 = 0.05$ typical of the experiments of Weidman and Maxworthy [9]. We note the strong similarity between the shapes of these KdV phase shifts curves and those for the diffusive two-pycnocline system shown in Figure 12.

4. Discussion and conclusion

The accurate numerical calculations of Nitsche et al. [1] for waves travelling on separate diffusive pycnoclines showed that a mode-two wave of elevation on one pycnocline is always accompanied by a phase-locked wave of depression on the neighboring pycnocline. This was part of the motivation for the study in Section 2—to see what combinations of parent and signature waves co-exist when the diffusive interfaces become sharp. Another reason for this study was to extend the extant results of Lamb [5] to the three-layer system and, in the

process, see if it corresponds to the results given in the Tripos exam paper detailed in the Appendix. Because the governing equation for the frequencies is bi-quadratic, it is not surprising to find that every parent wave on one pycnocline has two possible phase-locked signature waves on its neighboring pycnocline, one in-phase and the other out-of-phase with the parent wave. We indeed find that the Tripos result reduces to our frequency equation for the sharp three-layer system. The Tripos problem, however, does not give details about the amplitude ratios of the parent to its signature waves which are here determined explicitly. We provide these details and investigate under what conditions the parent and signature waves will have equal amplitudes, both for the in-phase and out-of-phase situations. Moreover, we show that equal amplitude signature waves cannot exist in a finite-depth system.

The second part of the study in Section 3 on the weakly nonlinear overtaking interaction of mode-two solitary waves in the diffuse two-pycnocline system shows that these waves are not solitons—the waves lose a minute amount of energy during the interaction which manifests itself in very small amplitude dispersive tails on both interfaces. Ultimately, the waves separate from their dispersive tails and evolve into distinct solitary waves. The curious feature is that the larger amplitude wave gains a very small amount of energy and the smaller wave loses considerably more energy as a result of the interaction. But these energies are indeed small, increasing up to 0.001% energy gained and 0.025% energy lost as the amplitude ratio increases from $\sigma = 1$ to $\sigma = 6$. The slight changes in wave amplitudes are attributed to the complicated interactions which occur in this system. The primary energy shift is the KdV upstream energy transfer along the same pycnocline, but there is also the LKK downstream energy transfer from one pycnocline to its neighboring pycnocline. One interesting combined energy transfer of this kind has been observed experimentally by Weidman & Johnson [3] in a three-wave interaction scenario.

The three types of KdV interactions discovered by Lax [8] are found for the example studied in detail. The values of the fluid depths, layer densities, and pycnocline thicknesses chosen for the example are those achievable in laboratory experiments, although such experiments have not been conducted to date. The spatial phase shifts exhibit features identical to those found in the KdV system: in absolute value the phase shift of the initially large-amplitude wave is smaller than that of the initially small-amplitude wave for all σ, with both decreasing monotonically with σ. Although no theory exists for this two-pycnocline solitary wave interaction on diffuse interfaces, it exhibits the Type I, II, and III interactions and appears, for all intents and purposes, to be a classic overtaking KdV interaction. Experimental verification of the small energy changes incurred by the interaction would be impossible, owing to the much larger viscous attenuation effects, and even in an electrical analog of the system one would be hard-pressed to observe such small energy differences.

However, our accurate numerical results show unequivocally that these solitary waves are not solitons.

Acknowledgments

The authors are grateful to Professor Tim Pedley for providing a duplicate copy of the Mathematical Tripos problem discussed in the Appendix.

Appendix: The Tripos Problem

In *Mathematical Tripos* Part III administered on Tuesday, January 18, 1884 the following multi-layer fluid problem was presented. The full problem definition is reproduced here below.

> xv. A rectangular pipe whose faces are horizontal and vertical planes is completely filled with $(n+1)$ fluids; show that the velocities of propagation of waves of length λ at the surfaces of separation of the strata are given by the equation

$$\begin{vmatrix} A_1 & -B_2 & \cdots & \cdots & \cdots & \cdots & \cdots & \cdots & \cdots \\ -B_2 & A_2 & -B_3 & \cdots & \cdots & \cdots & \cdots & \cdots & \cdots \\ \cdots & -B_3 & A_3 & -B_4 & \cdots & \cdots & \cdots & \cdots & \cdots \\ \cdots & \cdots & -B_4 & A_4 & -B_5 & \cdots & \cdots & \cdots & \cdots \\ \cdots & \cdots & \cdots & \cdots & \cdots & \cdots & \cdots & \cdots & \cdots \\ \cdots & \cdots & \cdots & \cdots & \cdots & \cdots & -B_{n-1} & A_{n-1} & -B_n \\ \cdots & \cdots & \cdots & \cdots & \cdots & \cdots & \cdots & -B_n & A_n \end{vmatrix} = 0,$$

> where $A_m = 2\pi v^2/\lambda(\rho_{m+1}\coth 2\pi h_{m+1}/\lambda + \rho_m \coth 2\pi h_m/\lambda) - g(\rho_{m+1} - \rho_m)$, $B_m = 2\pi v^2/\lambda \operatorname{cosech} 2\pi h_m/\lambda$, and h_m is the equilibrium thickness of the stratum ρ_m.
>
> In particular if $\rho_m = m\sigma$ and $h_m = ma$, then the $2n$ values of v are included in the formula

$$v = \pm\frac{1}{2}\sqrt{ga}\,\sec\left(\frac{m}{n+1}\frac{\pi}{2}\right),$$

> where m is supposed to assume the values 1, 2, 3,... n, and λ the wavelength is very large compared with na.

We now provide explicit results for two and three layers. For $m = 1$ the above equation reduces to $|A_1| = 0$ and making the identifications $V = c$,

$\sigma^2 = k^2c^2$ and $\lambda = 2\pi/k$, we obtain the result

$$\sigma^2 = \frac{kg\,(\rho_2 - \rho_1)}{\rho_2 \coth kh_2 + \rho_1 \coth kh_1}. \tag{A1}$$

This corresponds to one pair of roots of the equation given by Lamb [1, Section 2.31] for interfacial oscillations in the two-layer system. As noted by Lamb, *two* possible systems of waves of any given period is expected because the wavelength is prescribed. Note that further details of the problem, such as the upper/lower wave amplitude ratio, cannot be determined from the above Tripos solution, but intermediate results leading to that solution would provide this detail.

Now we consider $m = 2$ corresponding to the bounded three-layer system. In this case, the eigenvalue equation is determined by $|A_1A_2 - B_2^2| = 0$ in which

$$A_1 = \frac{\sigma^2}{k}[\rho_2 \coth kh_2 + \rho_1 \coth kh_1] - g(\rho_2 - \rho_1),$$

$$A_2 = \frac{\sigma^2}{k}[\rho_3 \coth kh_3 + \rho_2 \coth kh_2] - g(\rho_3 - \rho_2),$$

$$B_2 = \frac{\sigma^2}{k}\operatorname{cosech} kh_2.$$

Evaluation of the determinant and simplifying using the shorthand notations

$$\alpha = \frac{b}{a}, \qquad \beta = \frac{\sigma^2}{gk}, \qquad \gamma = \frac{\rho_1}{\rho_2}, \qquad \chi = \frac{\rho_3}{\rho_2}, \qquad \coth_n = \coth kH_n,$$

we arrive at our result given as Equation (18) when the Tripos h_n is identified with our H_n.

References

1. M. Nitsche, P. D. Weidman, R. Grimshaw, M. Ghrist, and B. Fornberg, Evolution of solitary waves in a two-pycnocline system, *J. Fluid Mech.* 642:235–277 (2010).
2. A. K. Liu, T. Kubota, and D. R. S. Ko, Resonant transfer of energy between nonlinear waves in neighbouring pycnoclines. *Studies Appl. Math.* 63:25–45 (1980).
3. P. D. Weidman and M. Johnson, Experiments on leapfrogging internal solitary waves. *J. Fluid Mech.* 122:195–213 (1982).
4. R. I. Joseph, Solitary waves in finite depth fluid. *J. Phys. A: Math. Gen.* 10:L225–L227 (1977).
5. H. Lamb, *Hydrodynamics*, Dover, New York, 1945.
6. R. Hirota, Exact solution of the Korteweg-de Vries equation for multiple collisions of solitons. *Phys. Rev. Lett.* 27:1192–1194 (1971).
7. G. B. Whitham, *Linear and Non-Linear Waves*, Wiley-Interscience, New York, 1974.

8. P. D. Lax, Integrals of nonlinear equations of evolution and solitary waves, *Comm. Pure. Appl. Math.* 21:467–490 (1968).
9. P. D. Weidman and T. Maxworthy, Experiments on strong interactions between solitary waves, *J. Fluid Mech.* 85:417–431 (1978).

University of Colorado
Univerity of New Mexico
Massachusetts Institute of Technology

(Received November 10, 2011)